Bifurcation Analysis of Bubble Dynamics in Fluidized Beds

Peter Blomgren, Antonio Palacios, Bing Zhu, Stuart Daw, Charles Finney, John Halow and Sreekanth Pannala

February 2007

Publication Number: CSRCR2007-08

COMPUTATIONAL SCIENCE & ENGINEERING

SAN DIEGO STATE UNIVERSITY

Computational Science Research Center
College of Sciences
5500 Campanile Drive
San Diego, CA 92182-1245
(619) 594-3430

Bifurcation Analysis of Bubble Dynamics in Fluidized Beds

Peter Blomgren[a],* Antonio Palacios[a],† and Bing Zhu[a,b]‡

[a] *Nonlinear Dynamical Systems Group,*

Department of Mathematics & Statistics,

San Diego State University, San Diego, CA 92182

[b] *San Diego Supercomputer Center, La Jolla, CA 92093-0505*

Stuart Daw[c],§ Charles Finney[c],¶ John Halow[d],** and Sreekanth Pannala[e]††

[c] *Engineering Science and Technology Division,*

Oak Ridge National Laboratory, Oak Ridge, TN 37831

[d] *Waynesburg College, Waynesburg, Pennsylvania 15370*

[e] *Computer Science and Mathematics Division,*

Oak Ridge National Laboratory, Oak Ridge, TN 37831

(Dated: January 8, 2007)

Abstract

We use a low-dimensional, agent-based bubble model to study the changes in the global dynamics of fluidized beds in response to changes in the frequency of the rising bubbles. The computationally based bifurcation analysis shows that at low frequencies, the global dynamics is attracted towards a fixed point since the bubbles interact very little with one another. As the frequency of injection increases, however, the global dynamics undergoes a series of bifurcations to new behaviors that include highly periodic orbits, chaotic attractors, and intermittent behavior between periodic orbits and chaotic sets. Using methods from time-series analysis, we are able to approximate nonlinear models that allow for long-term predictions and the possibility of developing control algorithms.

PACS numbers: 05.45.-a, 05.70.Ln, 47.11.+j

*Electronic address: `blomgren@terminus.sdsu.edu`

†Electronic address: `palacios@euler.sdsu.edu`

‡Electronic address: `bzhu@sdsc.edu`

§Electronic address: `dawcs@ornl.gov`

¶Electronic address: `finneyc@ornl.gov`

**Electronic address: `jhalow@waynesburg.edu`

[††]Electronic address: pannalas@ornl.gov

Keywords: Fluidization; Bubbles; Time-Series Analysis; Low-dimensional Model.

Fluidization is the phenomenon in which a bed of solid particles acquires fluid-like properties due to the interstitial upward flow of a fluid (typically gas) through the bed. Recent experimental and computational works have revealed that the hydrodynamics of fluidized beds exhibit many features associated with low-dimensional deterministic chaos. One particular regime of interest to this work is the bubbling fluidization regime in which gas is accumulated in pockets or "bubbles" that rise upward throughout the surrounding solids. In this work, we employ a previously published low-dimensional bubble model to simulate under controlled conditions the global behavior of bubbles as they rise through the bed. One of the control parameters is the injection frequency, and thus we seek to investigate the underlying bifurcations in the global dynamics in response to variations in injection frequency. We provide a qualitative and quantitative description, based on ideas and methods from nonlinear dynamics, of transitions in these dynamics. We hope this work can initially help improve the fundamental understanding of fluidized-bed dynamics and possibly later assist the development of improved control algorithms for fluidized-bed reactors.

I. BACKGROUND

Fluidization is a process in which solid particles are suspended in a fluid-like state by a carrier medium, typically air [1–4]. This phenomenon occurs when the drag forces on the particles from the upward fluid flow exceed gravitational and interparticle forces. Fluidized beds normally consist of a vessel containing the solids with a bottom porous plate through which the fluidizing medium, usually gas, can be introduced. At low fluid flow rates, the fluid percolates through the void spaces between the solids, which remains a packed bed; the forces acting on the bed due to the flow of the fluid is less than the weight of the bed. When the flow rate is increased over a certain threshold, known as the minimum fluidization velocity, the solids become levitated due to the interaction between the fluid and the particles, and the bed behaves like a fluid. Lighter particles float on top of the bed, the surface of the solids bed stays horizontal when its containment vessel is tilted (like water in a glass), and the solids can flow through an opening, such as a valve. This state is called fluidization.

If the rate of fluid flow is further increased beyond a second velocity threshold, bubble-shape voids form and rise through the bed with vigorous motion and extensive coalescence and splitting [5–9]. This state is called the bubbling fluidization regime, and the threshold velocity at which it first occurs is called the minimum bubbling velocity. The onset of bubble formation depends on the actual type and size of solid particles and on the particle/fluid density ratio. In a bed of coarse particles fluidized by a gas, for example, the onset of bubble formation is approximately the same as the minimum fluidization velocity. But regardless of when bubbles are formed, their vigorous motion, including coalescence and splitting, is important because they affect the efficiency of particle mixing. A bed with uniformly distributed fine bubbles, for instance, will generally lead to a higher chemical conversion than a bed containing a few large bubbles. If the fluid flow rate is increased beyond the terminal velocity of the particles, then the solids would be swept out of the container. If this material is captured and returned to the bed, then the unit is operating in the circulating fluidization regime.

Fluidized-bed reactors afford excellent gas-solid contacting and particle mixing, facilitate the control of highly exothermal reactions, and provide good gas-to-particle and bed-to-wall heat transfer. However, they also have disadvantages, such as a broad residence time distribution of the gas and particles, gas-bypassing in the form of gas bubbles, jets and channeling, the erosion of bed internals and the attrition of the bed material. Common engineering applications of fluidization technology include coal combustion, the production of polyethylene, and the cracking of hydrocarbons. Fluidization is in many ways related to the field of granular dynamics but offers a set of unique features and challenges because of the way the particles are agitated. For more information on the general engineering relevance of fluidization, please consult Ref. [10].

In the last decade, studies by Skrzycke *et al.* [11], Daw *et al.* [12, 13], Daw and Halow [14, 15], Schouten *et al.* [16–18], and vander Stappen *et al.* [19–21] have shown that the hydrodynamics of fluidized beds exhibit many features associated with low-dimensional deterministic chaos [22–24]. Then, in principle, one should be able to control the hydrodynamics of fluidization behavior by exploiting the sensitivity of the system to small perturbations. But the lack of realistic low-dimensional models for bubbling behavior has limited the progress of chaos-based control strategies.

Early attempts to develop such low-dimensional bubble models for fluidized beds were made first by Clift and Grace [6] and later by Halow and Daw [14]. These models focus on describing the wake interactions and coalescence processes among rising bubbles based on potential flow theory and empirical observations of bubble behavior in gas-liquid systems and bubbling fluidized beds. Later, Kaart *et al.* [25] and De Korte *et al.* [26] used such models to show how controlled gas injection into fluidized beds at precise times and locations can be used to modify the effectiveness of gas-solids contacting. Thus, in principle, they demonstrated that knowledge of the bubble dynamics can be exploited to improve the efficiency of fluidized-bed chemical reactors with nonlinear feedback.

More recently, Pannala *et al.* [27] have used this same type of model to study the collective interactions of large numbers of rising bubbles. We now recognize that this bubble model is actually a specific realization of a more general class of models referred to as self-propelled particle systems [28]. Such studies are needed in order to better understand how inherently high-dimensional systems consisting of large numbers of coupled components or "agents" are able to produce the low-dimensional dynamics (e.g., <6) seen in many experiments. For example, Pannala *et al.* were able to show that the Halow and Daw bubble model can reproduce collective swarming and avalanching processes that lead to large-scale intermittent collapses of bubble gas toward the center of the flow. These features now seem remarkably similar in a generic sense to that reported for locusts by Buhl *et al.* [28]. Bokkers *et al.* [29] have further improved the bubble models for fluidized beds to include the convection of the suspended solids (emulsion phase) as a continuity constraint so that the emulsion moves down as the bubbles move up. We anticipate that improvements of this kind will allow increasingly sophisticated studies of how real fluidized beds function and might be controlled.

In this work, we describe additional studies with the bubble model used by Pannala *et al.* [6] to understand the nature of the dynamics as they would be seen by an observer positioned at one location along a fluidized bed axis. We take this point of view because it is generally consistent with typical experimental observations and also dynamic measurements available in practical industrial situations. Key issues we seek to understand are:

a) What is the detailed nature of the local bifurcations produced as the rate of bubble injection is increased over a large range?

b) What is the effective dimensionality in the local dynamics as they would be seen by a typical observer?

c) What level of predictability should be expected based just on the local measurements as described above?

Our intention here is not to focus directly on the issue of fluidized-bed control (as did Kaart *et al.* [25] and De Korte *et al.* [26]) but rather to better understand the expected nature of the dynamical information that should be available to a typical experimental observer (at least what is predicted by this type of model). Of course such studies are relevant to control, but they also relate to more fundamental questions about the generation and transmission of information and self-organization in spatio-temporal systems.

Our simulated experimental measurement is a hypothetical laser detector that records the crossing time intervals of rising bubbles passing through the observing window. Previous experimental studies of bubble-train dynamics (e.g., the studies by Nguyen *et al.* [30] and Tufaile and Sartorelli [31, 32]) have successfully used this same type of measurement. Although the complete dynamical state space for a group of rising bubbles would have to account for each bubble's location and speed, experiments indicate that useful dynamical maps can be constructed from time-delayed versions of this simple type of localized measurement for bubble trains. Thus we adopt this same type of measurement to see what it reveals about the model.

The paper is organized as follows. In Section II we review the basic structure of the low-dimensional bubble model most relevant to this work. A complete description of the model can be found in [27]. In Section III we present numerical results of the observed bifurcations. Then we use time-series methods to reconstruct a discrete map that can characterize the complexity of the crossing-time measurements, in particular the underlying attractor of the global dynamics for various injection points.

II. THE LOW-DIMENSIONAL BUBBLE MODEL

The low-dimensional model, also known as the Dynamic Interacting Bubble Simulation (DIBS) model, was derived by Pannala *et al.* [27] under the simple assumption that each individual bubble can be treated as a dynamical "agent". Each bubble then rises according to its size and local conditions and coalesces when it comes in contact with neighboring bubbles. As each bubble rises and interacts, it also exchanges gas with the surrounding emulsion phase gas-solid mixture where most of the reactions proceed. All of the observed gas-solids mixing and reaction thus result from the collective effects of gas flowing smoothly upward through the emulsion phase and bubble gas flowing upward. In the remainder of this section, we summarize the basic principles of the DIBS model most relevant to this manuscript. For further details we refer interested readers to Pannala *et al.* [27].

The rise velocity of each bubble is based on an empirical correlation derived from capacitance imaging experiments [33]. The form of this correlation is based on earlier theoretical work by Davidson and Harrison [34] in which the motion of bubbles was modeled with potential flow analysis. The empirical correlation accounts for deviations from the rise behavior of single bubbles due to pairwise interactions between leading and trailing bubbles and wall effects. Each bubble's trajectory is described by integrating a first-order, nonlinear ordinary differential equation through time. Thus, if there are N bubbles in the bed, we use N equations to describe their motion. Bubbles are dynamically coupled through the dependence of each rise velocity on the distance to its closest leading neighbor, i.e., the nearest bubble above. This coupled system of equations for N bubbles can be written as:

$$\frac{d||X_i||}{dt} = ||V_i|| = \sqrt{\frac{g\,l_i}{2 + \left(\frac{A_i^*}{1 - A_i^*}\right)^2}} \left[1 + 3\left(\frac{D_{Lj}}{X_{i-j}}\right)^3\right]. \tag{1}$$

Referring to the i th bubble in the bed, V_i is its rise velocity, l_i is its length, A_i^* is the ratio of its cross-sectional area to that of the bed, D_{Lj} is the diameter of the bubble leading it, and X_{i-j} is the distance between bubble i and the bubble j leading it. The direction of X_i is taken to be along a line connecting the center of bubble i with the center of the bubble j that is leading it. If there is no leading bubble, the term D_{Li}/X_{i-j} is zero. A second key rule is that when bubbles touch, they coalesce to form a single bubble of equal total volume. Because of coalescence, the number of bubbles and thus the number of equations varies with time. In addition, bubbles entering and leaving the domain changes the number of equations in the system. While this constant shifting in the number of equations creates an unusual mathematical system with varying dimensionality, it is easy to handle numerically. Some of the key model assumptions that are most relevant to this work include:

i. The emulsion gas velocity actually exceeds the minimum fluidization velocity based on the experiments of Hilligardt and Werther [10]; this is a modified two-phase assumption.

ii. Bubbles are spherical if their diameters are less than or equal to 85% of the bed diameter. Larger bubbles are cylindrically shaped with hemispherical-end caps with diameters equal to 85% of the bed diameter.

iii. A bubble is a "trailing" bubble if it lies within the projected horizontal area defined by twice the diameter of its closest higher neighbor.

iv. Bubbles are formed at the distributor by accumulating gas in excess of the emulsion phase gas flow. The initial bubble diameter is calculated from an appropriate correlation for the type of distributor orifice or porous plate using the correlation [35], or it can be independently specified, e.g., according to a specified size distribution.

v. To simulate beds with porous-plate grids, the bubbles are placed at random locations on the grid. For grids with well-defined tuyeres or bubble caps, bubbles may be released randomly from these orifices or with specified frequencies.

vi. Bubbles exit the bed when their centers reach the bed surface.

vii. The bubble rise velocity is relative to the solids flow. Thus, the net solids downflow or upflow can be specified for standpipes and moving beds.

viii. Mass transfer is calculated based on the correlations developed by Kunii and Levenspiel [10]. More details are available in Pannala *et al.* [36].

Detailed comparison and validation of the DIBS model with experimental works can be found elsewhere [36].

III. ANALYSIS

A. Computational Bifurcation Diagrams

In this work, we use the DIBS model to investigate the underlying bifurcations that govern the transitions in the global dynamics of the rising bubbles in response to the injection frequency (denoted by f). Our assumed fluidized-bed configuration is illustrated in Fig. 1.

Both the central gas bubble injection and controlled injection rate are idealizations (compared to most practical fluidized beds) in order to simplify the problem. By controlling the bubble injection frequency explicitly (instead of allowing the bubbles to enter spontaneously), we can focus specifically on the dynamics of the bubbles once they have entered the bed itself. In future work, however, we will consider other injection scenarios such as multiple injection points with controlled injection frequency as well as spontaneous injection.

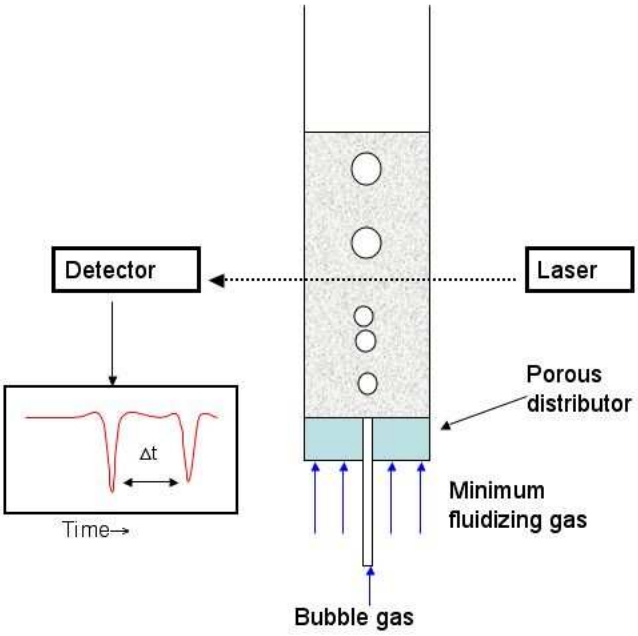

FIG. 1: Schematic of the fluidization-bed configuration assumed for our numerical experiment. Minimum fluidizing gas is injected through a porous distributor to levitate the solids, but the bubbles are produced by injecting pulses of additional gas through a central nozzle at a specified frequency. Bubbles passing an observation point above the distributor are detected by crossing a virtual laser beam.

To carry out the simulation, we have modified the DIBS flow chart (see Fig. 2) to make a virtual measurement of the intervening time interval between successive passages of bubbles as they pass through the observation point. Our objective is to capture the interaction between leading and traling bubbles through a low-dimensional discrete map. Details are provided later in Section III B. From a computational perspective, a significant change to the original flow chart is the utilization of an adaptive integration time, dt. Since injection frequency f is a linear product of the inverse product of number of bubbles, N, injected per integration time, i.e., $f = 1/(N \times dt)$, using an adaptive integration times allows us to conduct simulations over a refined grid of frequency values, even if the frequencies are not commensurate with the number of bubbles injected. In this way, the bifurcation diagram that we generate can exhibit the fine details of the global dynamics. Although the observation point is fixed for an individual simulation, we also investigate the effects of changing its location on the bifurcation diagram. The bed height is also assumed to be fixed at 40 cm. The modified DIBS code also accounts for changes in bubble injection frequencies, between the limit of almost zero up to 10 bubbles injected per second (we denote this injection frequency in Hz). In order to get insight into the underlying bifurcations, we consider only the case of a single central nozzle injector; the case of multiple injectors is deferred for future work.

We start the computer simulations with an observation point positioned at $h = 20\,\mathrm{cm}$, which is right in the middle height of the bed, and then measure the delay times, Δt_n, between successive bubbles crossing the observation point. To generate a well-defined bifurcation diagram, we use a 2000-grid over a frequency range $(0, 10]$ Hz. The original time-step size is set to 0.001 s. For each individual frequency, we let the program run for a minimum of 700 seconds, and in some cases up to 24000 seconds, in order to capture the long-term behavior. These computationally intensive jobs demand the use of *High Performance Computing*. Thus we have carried out all simulations at the *TeraGrid* machine at the San Diego Supercomputer Center, which provides a cluster of 102 teraflops of computing capability. Four computer nodes, IA-64 1.5 GHz per node, were used to run the simulations in parallel. Since each simulation (for a given frequency) is independent from the others, multiple batch jobs of bubbles simulation for different frequencies were launched by a Perl script, which is submitted four times into the four computer nodes. The computation time, for instance, for the 2000-grid on the zoomed-in frequency interval $[4, 6]$ is, approximately, 2.5 hours in each TeraGrid node. The exact number of bubbles that are being followed at a typical time varies with the injection frequency — about five bubbles for low frequencies and up to twenty bubbles for higher frequencies.

Fig. 3 depicts the resulting bifurcation diagram for this configuration with injection frequency varying from close to zero up to 10 Hz. At low injection frequencies, bubbles entering

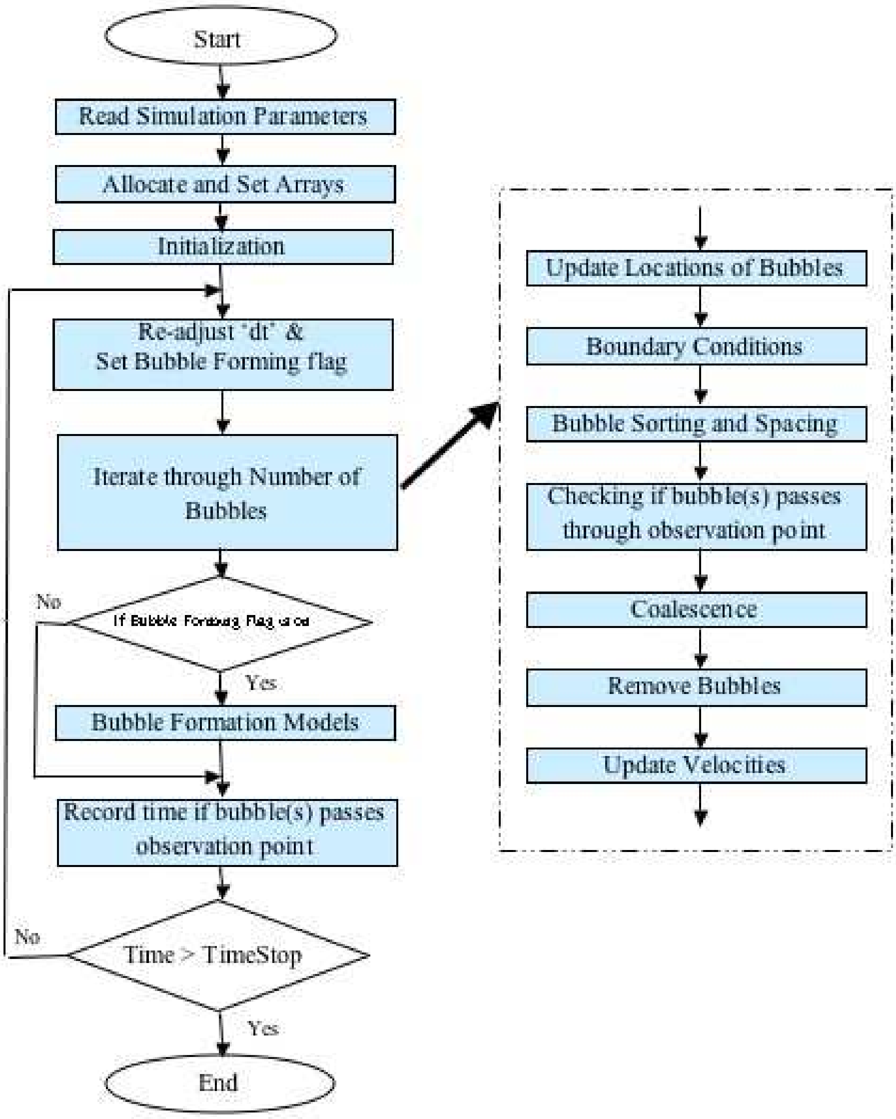

FIG. 2: Modified flow chart of the Dynamic Interacting Bubble Simulation model. The new model can now measure the passage times of bubbles through a predefined observation point in addition to simulating bubble interactions. Injection frequency is user-defined in the panel labeled "simulation parameters".

the bed are significantly separated and therefore their interaction is minimal, consequently they rise "almost" independently of each other. Thus, the global dynamics is attracted to a fixed point, as expected. As the injection frequency increases beyond $f = 4\,\mathrm{Hz}$, the global dynamics rapidly changes, however, from a fixed point to a region of quasi-periodic behavior that eventually becomes chaotic, then back to a more organized region of period-4 oscillations. Although it is hard to visualize under the scale of the graph, none of the crossing times is zero. The period-4 region bifurcates, at approximately $f = 4.7\,\text{Hz}$, into a region of intermittent behavior that involves four disjoint chaotic attractors. Near $f = 5\,\text{Hz}$, the chaotic attractors collide into a period-3 orbit that eventually changes into a period-2 orbit. A period-doubling bifurcation then leads to a period-4 orbit.

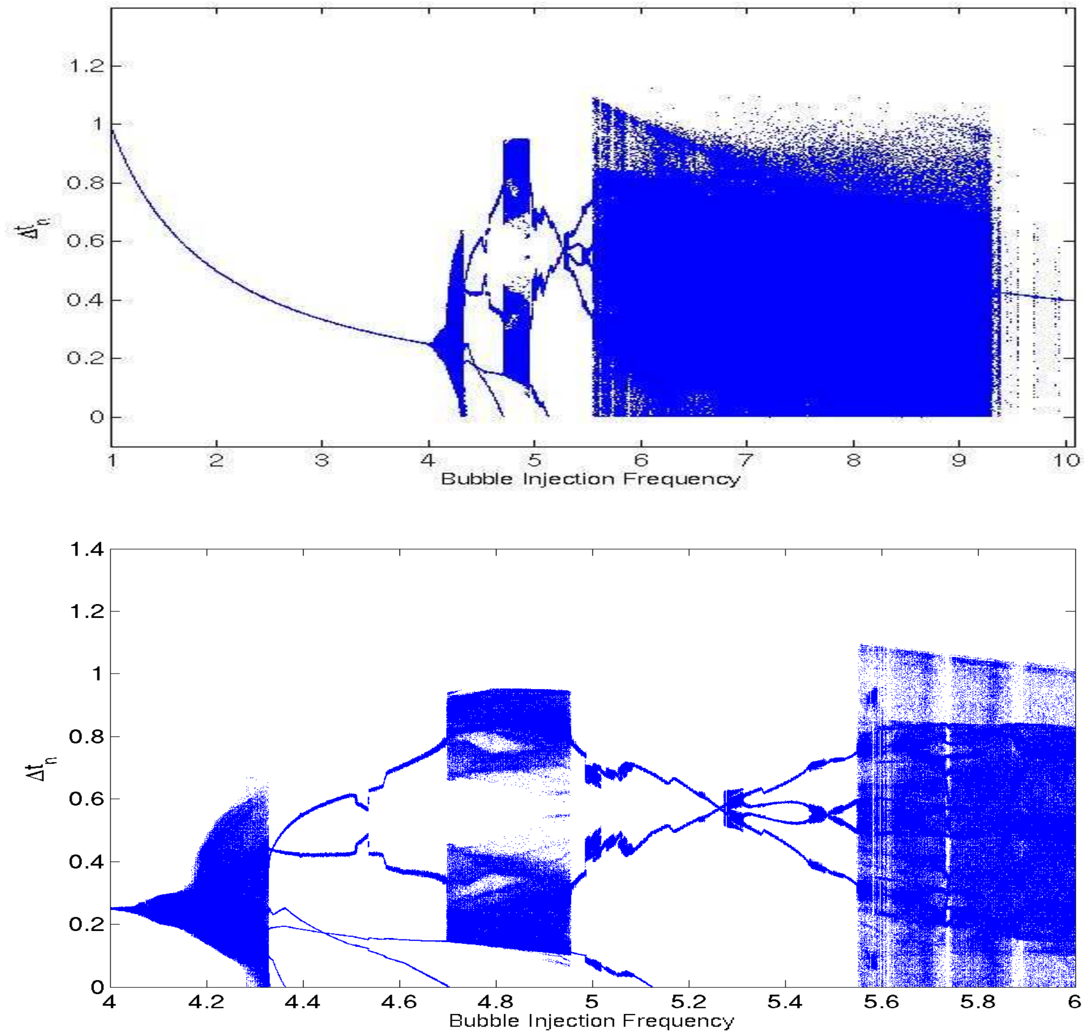

FIG. 3: Computational bifurcation diagram of time delay Δt_n between successive crossing bubbles as a function of injection frequency in a simulated fluidized bed with central nozzle injection. Bed height is $h = 40\,\text{cm}$ and observation point is set up at $h = 20\,\text{cm}$. (Top) Injection frequencies in the range $(0, 10]$ Hz. (Bottom) A close-up of injection frequencies in the range $[4, 6]$ Hz.

Beyond $f = 5.55\,\text{Hz}$, the system displays intermittent behavior in which the underlying dynamics randomly changes between a high-period orbit, approximately period-6, and a chaotic attractor as is shown in Fig. 4. This region of intermittent behavior persists until the injection frequency is large enough, at about $f = 9.25\,\mathrm{Hz}$, for the flow of bubbles to form an almost constant stream with little time to interact with one another so that the global dynamics is again attracted to a fixed point.

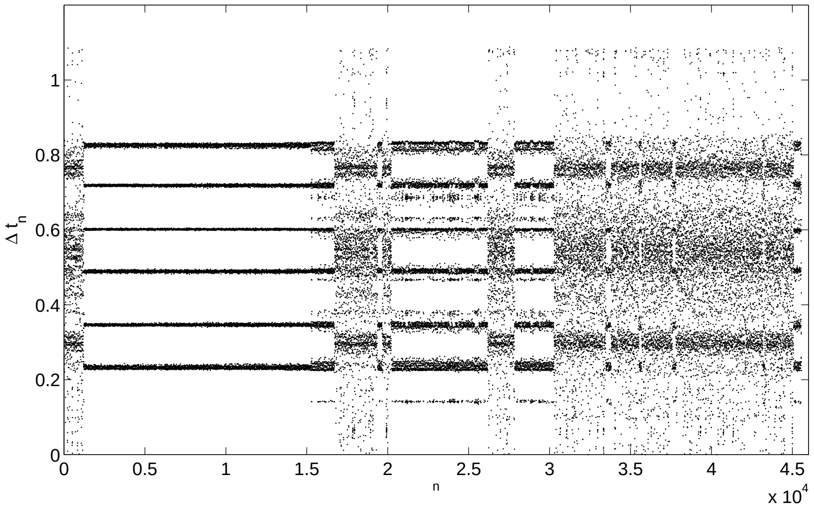

FIG. 4: 50000 iterations of the DIBS bubble model with bubble injection frequency of $f = 5.6\,\mathrm{Hz}$. At this frequency, the system displays intermittent behavior, in which the dynamics randomly changes between a period-6 orbit and a chaotic set.

B. Model Fitting

As noted in the Background section, the full state space for the DIBS bubble model would theoretically require sufficient dimensions to specify all of the positions and velocities of each bubble currently in the system. In the cases studied here, up to 20 bubbles were present in the bed at any one time, so the entire dynamical system would be represented by a 40-dimensional phase space (two ordinary differential equations for each bubble). (Note the number of equations actually shifts over time as bubbles leave the system or coalesce, presenting an interesting discontinuity.) However, we actually expect from the DIBS model that the local dynamics will be dominated by pairwise interactions between leading and trailing bubbles and also that the bubble stream will tend to collapse toward the bed center as the bubbles rise. This should tend to reduce the effective local dynamical dimension considerably.

Based on the above, it is reasonable to assume that the crossing times at the hypothetical laser detector are governed by the interactions between the crossing bubble at any given instant of time and the bubbles immediately above and below it. We would then expect the crossing dynamics to be described by a map of the form $\Delta t_{n+1} = G(\Delta t_n, \Delta t_{n-1})$, where Δt_n is the time interval between the n th and $(n+1)$ st crossing bubbles. That is, we expect the embedding dimension required to resolve the local dynamics to be close to a value of $d = 3$.

To check this expectation we used time-delay embedding of the observed crossing-interval time series to reconstruct the local attractor in the space $(\Delta t_n,\ \Delta t_{n-1},\ \ldots,\ \Delta t_{n-(d-1)})$ at various inlet bubble injection frequencies. We then estimated the minimal embedding dimension d through the method of false nearest neighbors [37], which yields the percentage of neighboring phase- space points that move apart as the embedding dimension increases. A minimal change in this percentage is indicative of a "good" estimate. Fig. 5 shows the result of applying the false nearest neighbors algorithm to the time-series data produced by the DIBS model with injection frequency 4.2 Hz. The percentage of nearest neighbors decreases monotonically as the embedding dimension increases, and the change is less than 0.1% when d changes from $d = 3$ to $d = 4$. It is then reasonable to assume that the required embedding dimension is $d = 3$. Similar results estimate the embedding dimension to be $d = 3$ for various values of injection frequency.

We note here that an embedding dimension of 3 appears to be within the range of experimental correlation-dimension values reported in the literature for bubbling fluidized beds, but it perhaps is somewhat on the low side of what might be expected. We speculate that this may be an indication that the model used here is missing some important dynamical components which might contribute to a higher effective dimensionality. If nothing else, the limitation of having only a single bubble injection location might be expected to reduce the resulting dimensionality.

Proceeding with an assumed embedding dimension of $d = 3$, we can write the time-delay vectors as $\Delta T_n = (\Delta t_n,\ \Delta t_{n-1},\ \Delta t_{n-2})$. In order to model the deterministic evolution of the time series data, we need a nonlinear map F of the form

$$\Delta T_{n+1} = F(\Delta T_n). \tag{2}$$

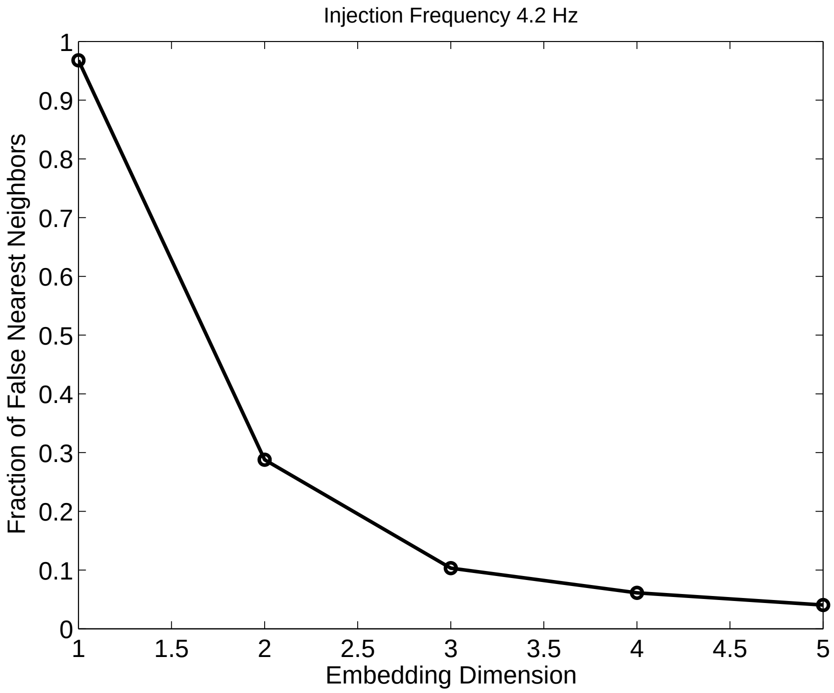

FIG. 5: Fraction of false nearest neighbors as a function of the embedding dimension for simulations of the DIBS bubble model with injection frequency of 4.2 Hz.

Since the observations Δt_n and Δt_{n-1} are common to both delay vectors ΔT_{n+1} and ΔT_n, we only need to find a map f for the last component of ΔT_{n+1}. That is, $\Delta t_{n+1} = f(\Delta T_n)$. The simplest case is to approximate f by a linear function of the form $f(\Delta T_n) = \vec{a}_n \cdot \Delta T_n + b_n$. The vector $\vec{a}_n$ and the scalar b_n are then found by minimizing the norm below

$$\sum_{i=1}^{M} ||\Delta t_{i+1} - \vec{a}_n \cdot \Delta t_i + b_n||^2,$$

with respect to $\vec{a}_n$ and b_n, M is the total number of time delay vectors. We have solved the minimization problem above with the aid of the TISEAN software package [38]. The linear fitting works very well for a wide range of frequencies up to $f = 4.55$ Hz. Fig. 6 shows (in green) the resulting time-delay representation of 1200 iterations of the DIBS model, at two representative values of injection frequencies: 4.2 Hz and 4.8 Hz. In black, we show iterations from the local linear model. Beyond $f = 5.55$ Hz, where the system exhibits intermittency between periodic orbits and chaotic attractors, both approximations, local linear fitting and global nonlinear multivariate polynomial fitting, fail to produce adequate long-term predictions.

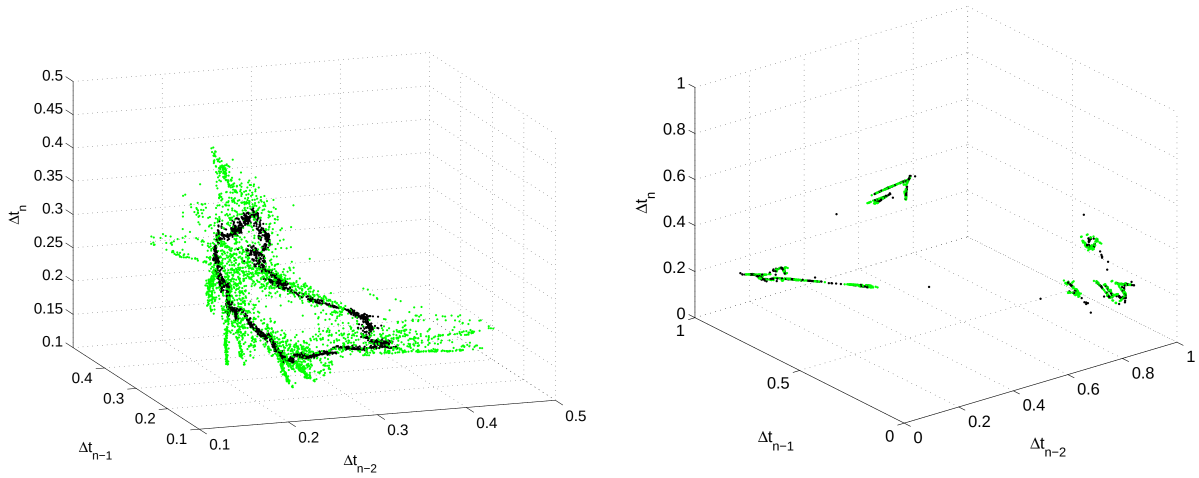

(a) $f = 4.2\,\mathrm{Hz}$ (b) $f = 4.8\,\mathrm{Hz}$

FIG. 6: (Color online) Time-delay representations of 1200 iterations of (green) the DIBS bubble model and of (black) a local linear predictor, for two representative values of injection frequency.

Next we quantify the rates at which neighboring orbits on each individual attractor, for each injection frequency, diverge (or converge) as the time-passage dynamics evolves in time through the following equation:

$$\lambda \approx \frac{1}{n} \ln \left| \frac{F^n(\Delta T_0 + \varepsilon_0) - F^n(\Delta T_0)}{\varepsilon_0} \right| \tag{3}$$

where ε_0 is an arbitrary small perturbation of the bubble dynamics. Equation (3) is an estimate of the largest Lyapunov exponent; it represents the rate of growth or decay of small perturbations along the principal axes of the system's state space. In practice, we apply (3) to an ensemble of orbits and then we average them to obtain a more statistically meaningful measure of Lyapunov exponents. Figure 7 shows the estimated Lyapunov exponents for a wide range of injection frequencies. Observe that the sign of the exponent agrees with the attractor depicted by the bifurcation diagram. That is, for low frequencies, the largest exponent is negative, indicating convergence towards the fixed point, as is normally observed in laboratory experiments as well as in our simulations of the DIBS model. For intermediate frequencies, between $f = 4$ and $f = 5.55\,\mathrm{Hz}$, the sign of the largest exponents randomly changes from negative to positive. A positive Lyapunov exponent is indicative of deterministic chaotic behavior in the passage-time dynamics because the time-series measurements of crossing times are bounded by the maximum passing time of a bubble rising all the way from the injection point to the top of the bed. More precisely, an upper bound of crossing times is $H_{\max}/||V_i||_{\min} + 1/f$, where $H_{\max}$ is the height of the bed, f is the injection frequency, and $||V_i||_{\min}$ is the minimum rising velocity given by

$$||V_i||_{\min} = \sqrt{\frac{g\, l_i}{2 + \left(\frac{A_i^*}{1-A_i^*}\right)^2}}.$$

For frequencies larger than $f = 5.55\,\mathrm{Hz}$, the sign of the largest exponent is mainly positive. In this region, however, the time-passage dynamics is not only chaotic but rather intermittent, randomly switching between chaotic attractors and high-period orbits. Observe also that the largest Lyapunov exponent is zero at the points of bifurcation where the system dynamics changes behavior.

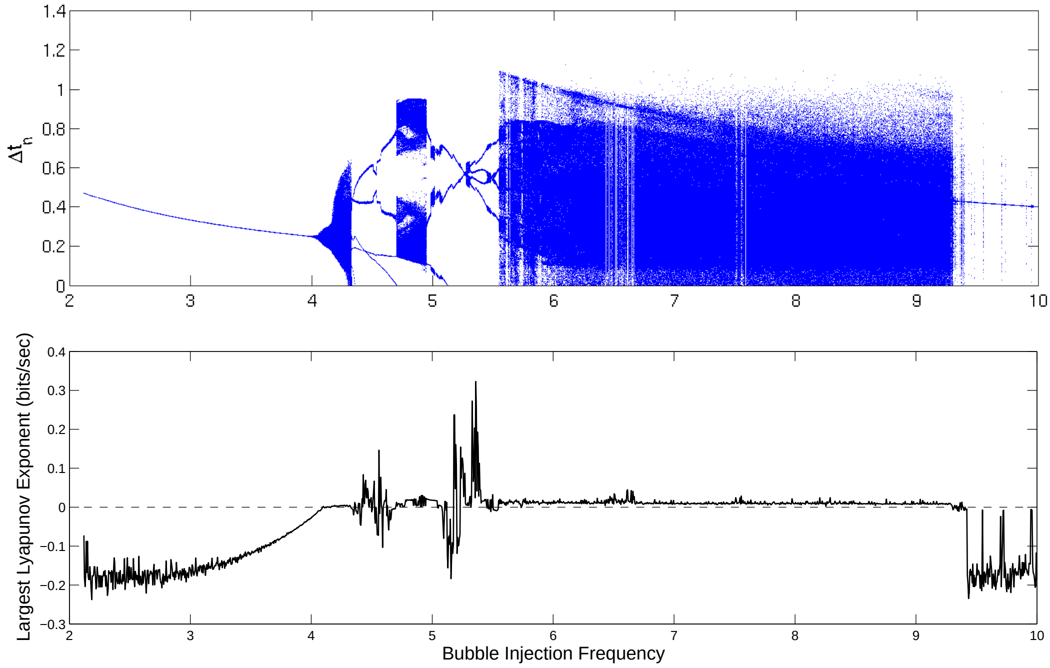

FIG. 7: Largest Lyapunov exponent of time-series bubble dynamics for various values of injection frequencies. A positive exponent is indicative of chaotic behavior in the system's dynamics.

The presence of the intermittency in the bifurcation sequence is likely to be difficult to ever see experimentally because of the presence of parametric noise (e.g., from gas-flow turbulence or granular particle flow). Such noise would be expected to continually stimulate intermittent jumps in these areas of the bifurcation sequence, thus causing the periodic features to be blurred into an apparent broad band of chaos. This suggests that future bifurcation studies of such bubble models should also consider the impact of realistic levels of parametric noise to the system.

IV. SUMMARY

We have used a low-dimensional, multi-agent model of bubbles in gas-fluidized beds to investigate the bifurcations that underlie their global dynamics in response to changes in the frequency at which they rise and interact with one another. This study was aimed at the relatively simple case of bubble injection through a central nozzle. As a measurement variable we employ the time of passage of successive bubbles through an observation point located at a predefined height within the fluidized bed.

The resulting bifurcation diagrams show that at low frequencies, the global dynamics is attracted towards a fixed point since the bubbles interact very little with one another, so passage times remain fairly constant. As the frequency of injection increases, however, the passage-time dynamics undergo a series of bifurcations to new behavior that include highly periodic orbits, chaotic attractors, and intermittent behavior between periodic orbits and chaotic sets. Except for the intermittent regime, we were able to approximate nonlinear models that allow for long-term predictions and the possibility of developing future control algorithms. The occurrence of this intermittent regime suggests that there are certain flow conditions for which control may be extremely difficult. Changing the observation point leads to qualitatively similar results, though with lower observation points we find a greater tendency of the global dynamics towards orbits of higher period, as is shown in Fig. 8.

We also wish to emphasize that the use of High Performance Computing at the San Diego Supercomputer Center was instrumental to help us carry out the computationally intensive simulations of the DIBS model and to help us achieve bifurcation diagrams with very high resolution. Work in progress includes an extension of the current analysis to the more realistic scenario of multiple injection points with simultaneous, random injection times, and parametric noise. For such work, we are considering parallelization of the bubble simulation code through the TeraGrid facilities.

V. ACKNOWLEDGMENTS

We would like to thank the Computational Science Research Center at SDSU for their technical support and the San Diego Supercomputer Center for providing us access to their TeraGrid facilities. We also wish to thank Ricardo Carretero for helpful discussions. The

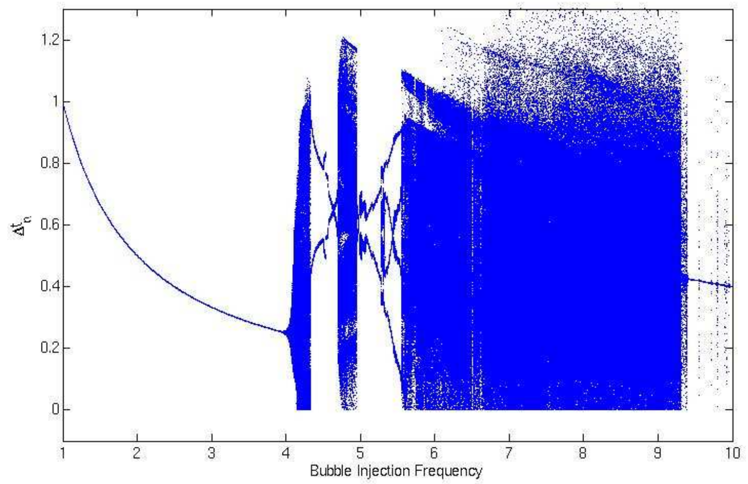

(a)Observation point $h = 30$ cm

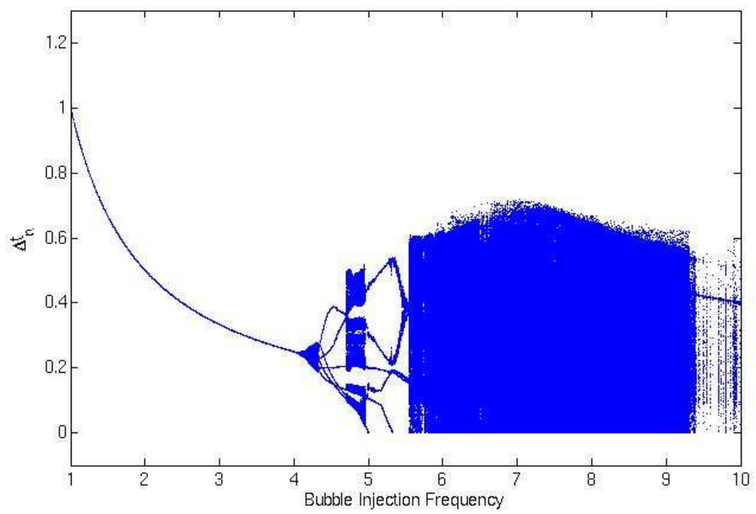

(b)Observation point $h = 10$ cm

FIG. 8: Bifurcation diagrams generated at two other observation points, $h = 10$ cm and $h = 30$ cm. As the observation point decreases the global dynamics exhibits greater tendency towards orbits of higher period.

NOMENCLATURE

g	Acceleration of gravity
h	Instantaneous bed height
l_i	Length of the i th bubble
t	Time
Δt_n	Time between successive bubble crossings of the observation point
d	Emedding dimension
f	Frequency of bubble injection
A_i^*	$=(D_i/D_t)^2 =$ (cross-sectional area of i th bubble/cross-sectional area of bed)
A_{bed}	Area of bed
A_r	Cross-sectional area of the bubble stream (area based on radius of gyration)
A_r^*	Normalized cross-sectional area of the bubble stream (A_r/A_{bed})
D	Diameter of the bubble
D_i	Diameter of the i th bubble
D_t	Diameter of fluidized bed
D_{Li}	Diameter of bubble leading i th bubble in bed
H_{bed}	Fixed bed height of the bed
H_{max}	Maximum height of the bed
N	Number of bubbles in the bed at time t
V_i	Velocity of the i th bubble
$\mathbf{X}_i$	Position of center of the i th bubble
X_{i-j}	Distance between the center of the i th bubble and the bubble leading it, L_i
dt	Time step for integration

[1] L.S. Fan and C. Zhu. *Principles of Gas-Solid Flows*. Cambridge University Press, New York, 1998.

[2] S.K. Garg and J.W. Pritchett. Dynamics of gas-fluidized beds. *Journal of Applied Physics*, 46:4493–4500, 1975.

[3] D. Gidaspow. *Multiphase Flow and Fluidization*. Academic Press, Boston, 1994.

[4] D. Gidaspow and B. Ettehadieh. Fluidization in two-dimensional beds with a jet; part 2: Hydrodynamic modeling. *Ind. Engng. Chem. Fundam.*, 22:193–201, 1983.

[5] A. Boemer, H. Qi, and U. Renz. Eulerian simulation of bubble formation at a jet in a two-dimensional fluidized bed. *Int. J. Multiphase Flow*, 23(5):927–944, 1997.

[6] R. Clift and J.R. Grace. Bubble interaction in fluidized beds. *Int. J. Multiphase Flow*, 105:14–27, 1985.

[7] D. Gera and M. Gautam. Variation of throughflow velocity in a 2-D rising bubble. *Powder Tech.*, 79(3):257–263, 1994.

[8] D. Gera and M. Gautam. Bubble rise velocity in two-dimensional fluidized beds. *Powder Tech.*, 84(3):283–285, 1995.

[9] F.A. Zenz. Bubble formation and grid design. *Instn. Chem. Engng. Symp. Ser.*, 30:136–139, 1968.

[10] D. Kunii and O. Levenspiel. *Fluidization Engineering*, 2nd ed., Butterworth-Heinemann, Boston 1991.

[11] D.P. Skrzycke, K. Nguyen, and C.S. Daw. Characterization of the fluidization behavior of different solid types based on chaotic time series analysis of pressure signals. In *Proceedings of the 12th International Conference on Fluidized Bed Combustion*, pages 155–156, San Diego, California, 1993.

[12] C.S. Daw, C.E.A. Finney, M. Vasudevan, N.A. van Goor, K. Nguyen, D.D. Bruns, E.J. Kostelich, C. Grebogi, E. Ott, and J.A. Yorke. Self-organization and chaos in a fluidized bed. *Phys. Rev. L*, 75:2308–2311, 1995.

[13] C.S. Daw, W.F. Lawkins, D.J. Downing, and N.E. Clapp Jr. Chaotic characteristics of a complex gas-solids flow. *Phys. Rev. A*, 41:1179–1181, 1990.

[14] C.S. Daw and J.S. Halow. Modeling deterministic chaos in gas-fluidized beds. *AIChE Sympo-*

sium Series Fluidized Processes: Theory and Practice, A. Weimer, ed., 88(289), 61-69 (1992).

[15] C.S. Daw and J.S. Halow. Evaluation and control of fluidization quality through chaotic time series analysis of pressure-drop measurements. *AIChE Symposium Series*, 1993.

[16] J.C. Schouten and C.M. van den Bleek. Chaotic hydrodynamics of fluidization: consequences for scaling and modeling of fluidized bed reactors. *AIChE Symposium Series*, 1992.

[17] J.C. Schouten, M.L.M. van der Stappen, and C.M. van den Bleek. Deterministic chaos analysis of gas-solids fluidization. In O.E. Potter and D.J. Nicklin, editors, *Fluidization VII*, pages 103–111, New York, 1992. Engineering Foundation.

[18] C.M. van den Bleek and J.C. Schouten. Deterministic chaos: A new tool in fluidized bed design and operation. In *Chemical Engineering Journal and Biochemical Engineering*, 53(1), 75-87 (1993).

[19] M.L.M. van der Stappen, C. Schouten, and C.M. van den Bleek. Application of deterministic chaos theory in understanding the fluid dynamic behavior of gas-solids fluidization. *AIChE Symposium Series*, 1993.

[20] M.L.M. van der Stappen, C. Schouten, and C.M. van den Bleek. The gas-solids fluidized bed as a spatio-temporal chaotic system. *AIChE Symposium Series*, 1994.

[21] M.L.M. van der Stappen, C. Schouten, and C.M. van den Bleek. Chaotic hydrodynamics and scale-up of gas-solids fluidized beds: using the Kolmogorov entropy for quantification. In *Fluidization VIII*. Engineering Foundation, 1995.

[22] R. Bakker, R.J. de Korte, J.C. Schouten, F. Takens, and C.M. van den Bleek. Neural networks for prediction and control of chaotic fluidized bed hydrodynamics: a first step. *Fractals*, 1997.

[23] R. Bakker, J.C. Schouten, M.O. Coppens, F. Takens, and C.M. van den Bleek. Robust learning of chaotic attractors. In S.A. Solla, T.K. Leen, and K.R. Miller, editors, *Advances in Neural Information Processing Systems*, volume 12, pages 879–885, Cambridge, 2000. MIT Press.

[24] R. Bakker, J.C. Schouten, C.L. Giles, F. Takens, and C.M. van den Bleek. Learning chaotic attractors by neural networks. *Neural Computation*, 2000.

[25] S. Kaart, J.C. Schouten, and C.M. van den Bleek. Improving conversion and selectivity of catalytic reactions in bubbling gas-solid fluidized bed reactors by control of the nonlinear bubble dynamics. *Catalysis Today*, **48**, 185–194 (1999).

[26] R.J. de Korte, J.C. Schouten, C.M. van den Bleek. Controlling bubble coalescence in a mechanistic fluidized bed model using bubble injection. *AIChE J.*, **47**, No. 5, 851–860 (2001).

[27] S. Pannala, C.S. Daw, and J.S. Halow. Dynamic interacting bubble simulation (DIBS): An agent-based bubble model for reacting fluidized beds. *Chaos, Focus Issue*, **14**, No. 2., 487-498 (2004).

[28] J. Buhl, D.J.T. Sumpter, I.D. Couzin, J.J. Hale, E. Despland, E.R. Miller, S.J. Simpson. From Disorder to Order in Marching Locusts. *Science*, **312**, 1402–1406 (2006).

[29] G.A. Bokkers, J.A. Laverman, M. van Sint Annaland, and J.A.M. Kuipers. Modelling of large-scale dense gas-solid bubbling fluidised beds using a novel discrete bubble model. *Chem. Eng. Sci.*, 61:5590-5602, 2006.

[30] K. Nguyen, P. Chakka, M. Cheng, C.E.A. Finney, D.D. Bruns, and C.S. Daw, and M.B. Kennel. Spatio-temporal dynamics in a train of rising bubbles. *Chemical Engineering Journal*, **64**, No. 1, 191–197 (1996).

[31] A. Tufaile and J.C. Sartorelli. Chaotic behavior in bubble formation dynamics. *Physica A*, **275** No. 3–4, 336–346 (2000).

[32] A. Tufaile and J.C. Sartorelli. Henon-like attractor in air bubble formation. *Physics Letters A*, **275**, 211-217 (2000).

[33] J.S. Halow, G.E. Fasching, and P. Nicoletti. Observations of a fluidized bed using capacitance imaging. *Chem. Eng. Sci.* **48**, 643 (1992).

[34] J. Davidson and D. Harrison. *Fluidized Patterns*, Cambridge University Press, Cambridge 1963.

[35] S. Mori and C.Y. Wen. Estimation of bubbles diameter in gaseous fluidized beds. *AIChE J.* **21**, 109 (1975).

[36] S. Pannala, C.S. Daw, and J.S. Halow. Simulation of reacting fluidized beds using an agent-based bubble model. *Int. J. Chem. Reactor Eng.*, **1** A20 (2003).

[37] M.B. Kennel, R. Brown, and H. Abarbanel. Determining embedding dimension for phase-space reconstruction using a geometrical construction. *Phys. Rev. A* **45**, 3403 (1992).

[38] R. Hegger and H. Kantz. Practical implementation of nonlinear time series methods: The TISEAN package. *Chaos*, **9**, no. 2., 413-435 (1999).